Why Are Eddy Fluxes of Potential Vorticity Difficult to Parameterize?

CHRIS WILSON AND RICHARD G. WILLIAMS

Oceanography Laboratories, Department of Earth and Ocean Sciences, University of Liverpool, Liverpool, United Kingdom

(Manuscript received 14 August 2002, in final form 11 April 2003)

ABSTRACT

Eddy fluxes systematically affect the larger-scale, time-mean state, but their local behavior is difficult to parameterize. To understand how eddy fluxes of potential vorticity (PV) are controlled, the enstrophy budget is diagnosed for a five-layer, 1/16°, eddy-resolving, isopycnic model of a wind-driven, flat-bottom basin. The direction of the eddy flux across the mean PV contours is controlled by the Lagrangian evolution of enstrophy, including contributions from the temporal change and mean and eddy advection, as well as dissipation of enstrophy. During the spinup, an overall increase in enstrophy is consistent with eddy fluxes being directed downgradient on average and homogenization of PV within intermediate layers. Enstrophy becomes largest along the flanks of the gyre, where PV gradients are large, and becomes smallest in the interior. At a statistically steady state, there is a reversing pattern of up- and downgradient eddy PV fluxes, which are locally controlled by the advection of enstrophy. A downgradient eddy PV flux occurs only on the larger scale over the gyre flanks and part of the western boundary. These larger-scale patterns are controlled by the eddy advection of enstrophy, which becomes significant in regions of high eddy enstrophy. As a consequence, at a statistically steady state, the eddy PV fluxes are not simply related to the mean fields, and their local, finescale pattern is difficult to parameterize.

1. Introduction

The atmosphere and ocean contain energetic eddy circulations that affect the time-mean circulation through their transfer of heat and dynamic tracers, such as potential vorticity (hereinafter PV). In the ocean, eddy stirring leads to the homogenization of PV within closed geostrophic contours (Rhines and Young 1982a,b), as obtained within unforced layers of eddy-resolving models above flat topography. This homogenization is consistent with diagnostics of nearly uniform PV over the upper ocean (McDowell et al. 1982; Keffer 1985). Eddy fluxes of PV have been parameterized in terms of a downgradient PV closure (e.g., Rhines and Holland 1979; Marshall 1984). In addition, eddies provide a transport of tracers within isopycnic layers (Gent et al. 1995); for a model illustration, see Lee et al. (1997). Eddy transport has also been interpreted in terms of downgradient closures in layer thickness (Gent and McWilliams 1990; Visbeck et al. 1997) or PV (Treguier et al. 1997; Killworth 1997; Greatbatch 1998; Marshall et al. 1999).

Despite the important role of eddies in determining the time-mean state, it is unclear whether these eddy parameterization schemes invoking layer thickness or PV closures have any local skill. Model comparisons of resolved eddy fluxes with parameterization schemes only generally show at best a weak correlation (e.g., Roberts and Marshall 2000; Drijfhout and Hazeleger 2001), unless there are special symmetries in the flow (Visbeck et al. 1997; Marshall et al. 1999). In this study, we address this paradox of why eddy fluxes do *not* significantly correlate locally with time-mean variables while the eddy fluxes still have a systematic effect on the evolution of the time-mean state. Here, we examine how the eddy fluxes of PV are controlled in terms of the enstrophy budget, extending previous studies by Rhines and Holland (1979), Holland and Rhines (1980), Marshall and Shutts (1981), and Marshall (1984).

In section 2, a theoretical context is provided discussing the eddy enstrophy budget (hereinafter referred to as enstrophy) for an isopycnal layer and retaining all high-order terms. The component of the eddy PV flux perpendicular to PV contours is determined by the Lagrangian evolution, and the local dissipation, of enstrophy. This Lagrangian evolution includes contributions from the local temporal change, as well as the mean and eddy advection of enstrophy. The mechanism by which the eddy PV flux and the eddy advection of enstrophy is fundamentally connected is illustrated. In section 3, PV and enstrophy diagnostics are performed for an eddy-resolving, isopycnic model of a classical, wind-forced, flat-bottom basin. Our diagnostics complement previous layered model studies for a basin by Drijfhout

Corresponding author address: Dr. Richard G. Williams, Oceanography Laboratories, Department of Earth and Ocean Sciences, University of Liverpool, Liverpool L69 7GP, United Kingdom.
E-mail: ric@liv.ac.uk

and Hazeleger (2001) and Peterson and Greatbatch (2001). The PV and enstrophy distributions are examined during the spinup and at a statistically steady state, including diagnostics of the time-mean advective and flux forms of the enstrophy budget. In section 4, the implications of the study are discussed.

2. Eddy PV flux and the enstrophy budget

In principle, the direction of the eddy flux of PV across time-mean contours of PV can be diagnosed from the general enstrophy equation:

$$\overline{\frac{D}{Dt}\frac{Q'^2}{2}} + \overline{\mathbf{u}'Q'} \cdot \nabla\overline{Q} = \overline{F'Q'}, \tag{1a}$$

or equivalent,

$$\overline{\frac{\partial}{\partial t}\frac{Q'^2}{2}} + \overline{\overline{\mathbf{u}} \cdot \nabla\frac{Q'^2}{2}} + \overline{\mathbf{u}' \cdot \nabla\frac{Q'^2}{2}} + \overline{\mathbf{u}'Q'} \cdot \nabla\overline{Q} = \overline{F'Q'}. \tag{1b}$$

This relation is derived in the appendix with terms involving third- and higher-order correlations of eddy fields retained and flux version included. Here, $Q'^2/2$ is the enstrophy (one-half of the variance of the PV), $D/Dt = \partial/\partial t + \mathbf{u} \cdot \nabla$, Q is the PV (Ertel or quasigeostrophic), F represents the forcing and dissipation of PV, and $\mathbf{u}$ is the three-dimensional velocity. The overbar represents a mean over many eddy periods, and the prime represents a deviation from the mean.

In (1a), the scalar product of the eddy PV flux and time-mean PV gradient (second term) is controlled by the mean Lagrangian change of enstrophy (first term) and the forcing of enstrophy (third term) by frictional, viscous, and diabatic processes. The mean Lagrangian change of enstrophy includes contributions from the mean and eddy advection of enstrophy, $\overline{\overline{\mathbf{u}} \cdot \nabla(Q'^2/2)}$ and $\overline{\mathbf{u}' \cdot \nabla(Q'^2/2)}$, respectively, in (1b).

If enstrophy is dissipated and advection of enstrophy is unimportant, then a downgradient eddy PV flux occurs [(1a)]. In practice, there are spatial variations in the enstrophy distribution over a basin, which can affect the direction of the eddy PV flux through correlations with the velocity field. Previous studies, such as Holland and Rhines (1980) and Marshall and Shutts (1981), have concentrated on how the advection of enstrophy by the mean flow can alter the sign of the eddy PV flux. In this study, we emphasize how the eddy PV flux is directed downgradient when there is a downstream increase in enstrophy following the flow that includes both a mean and eddy contribution.

Connection between the eddy PV flux and eddy advection of enstrophy

The direction of the eddy PV flux is revealed by considering the scalar product of the eddy PV flux and PV gradient, $\mathbf{u}'Q' \cdot \nabla Q$, which can be expressed in terms of a time-mean contribution and eddy advection of enstrophy,

$$\begin{aligned}\mathbf{u}'Q' \cdot \nabla Q &\equiv \mathbf{u}'Q' \cdot \nabla\overline{Q} + \mathbf{u}'Q' \cdot \nabla Q' \\ &\equiv \mathbf{u}'Q' \cdot \nabla\overline{Q} + \mathbf{u}' \cdot \nabla\frac{Q'^2}{2}.\end{aligned} \tag{2}$$

These contributions can either reinforce or oppose each other. To understand the connection between the eddy PV flux and eddy advection of enstrophy, consider the following two limits.

1) IDEALIZED PERTURBATION DURING A SPINUP

During a spinup, there is a temporal change in the PV and enstrophy distributions, which is partly achieved by the eddy fluxes. Consider an instantaneous Q contour, which is perturbed along a zonal channel from time-mean zonal $\overline{Q}$ contours (full and dashed lines, respectively, in Fig. 1). The oscillation is drawn such that there is a downgradient eddy PV flux, $v'Q' < 0$, because $v' > 0$ and $Q' = Q - \overline{Q} < 0$ on the left-hand side and $v' < 0$ and $Q' > 0$ on the right-hand side of Fig. 1.

There is a band of high enstrophy along the center of the channel, associated with the deviation of the instantaneous Q contour (shaded in Fig. 1), and there are zero values along the northern and southern boundaries. The velocity perturbation is drawn such that there is an eddy advection of enstrophy, $v'\partial/\partial y(Q'^2/2) < 0$, because v' and $\partial/\partial y(Q'^2/2)$ have opposite signs over the channel [where $\partial/\partial y(Q'^2/2)$ is evaluated where the velocity vector is marked between the central disturbance and the nearest boundary]. In this case, both $v'Q'\partial\overline{Q}/\partial y$ and $v'\partial/\partial y(Q'^2/2)$ reinforce each other, and, more general,

$$\mathbf{u}'Q' \cdot \nabla Q \equiv \mathbf{u}'Q' \cdot \nabla\overline{Q} + \mathbf{u}' \cdot \nabla\frac{Q'^2}{2} \neq 0. \tag{3a}$$

Whether both terms are significant depends on the length scales over which $\overline{Q}$ and Q' vary (which is explored further in section 3).

2) STATISTICALLY STEADY STATE

At a statistically steady state, the temporal change in the PV and enstrophy distributions becomes small. As a consequence, the eddy PV flux can become directed along instantaneous PV contours, rather than across them. Thus (2) reduces to $\mathbf{u}'Q' \cdot \nabla Q \simeq 0$, and

$$\mathbf{u}' \cdot \nabla\frac{Q'^2}{2} + \mathbf{u}'Q' \cdot \nabla\overline{Q} \simeq 0. \tag{3b}$$

These two limits are explored further in the subsequent eddy-resolving diagnostics in section 3.

3. Eddy-resolving model diagnostics

a. Model formulation

The relationship between enstrophy distributions and PV fluxes is examined using eddy-resolving integrations

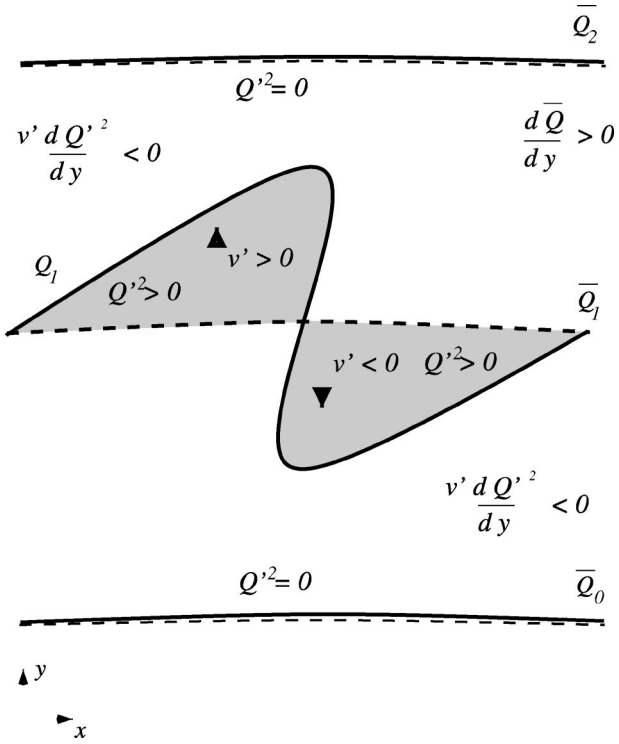

FIG. 1. Schematic figure that depicts the relationship between the eddy PV flux and eddy advection of enstrophy during spinup. A wavelike perturbation is considered with a perturbation velocity (vectors) and deviations in the instantaneous PV contour Q_1 (full line) along the center of a channel relative to zonal time-mean PV contours (dashed lines). The perturbation is drawn such that there is a downgradient eddy PV flux, $v'Q' < 0$, relative to the northward mean PV gradient, $d\overline{Q}/dy > 0$, giving $v'Q'd\overline{Q}/dy < 0$ (where $\overline{Q_2} > \overline{Q_1} > \overline{Q_0}$). Here, the shaded region on the left has $Q' = Q - \overline{Q} < 0$ and the shaded region on the right has $Q' > 0$ (assuming that the PV below Q_1 has values between $\overline{Q_0}$ and $\overline{Q_1}$ and that the PV above Q_1 has values between $\overline{Q_1}$ and $\overline{Q_2}$). In both shaded regions there is high enstrophy, $Q'^2 > 0$, whereas $Q'^2 = 0$ to the far north and south. Thus, in the regions of a velocity perturbation, $v'd(Q'^2)/dy < 0$, because in the shaded regions between the dashed lines $\overline{Q_1}$ and $\overline{Q_2}$, $d(Q'^2)/dy < 0$, and between $\overline{Q_0}$ and $\overline{Q_1}$, $d(Q'^2)/dy > 0$. During a spinup, the sign of these terms are consistent with $\mathbf{u}'Q' \cdot \nabla\overline{Q}$ and $\mathbf{u}' \cdot \nabla Q'^2/2$ reinforcing each other.

of a five-layer, 1/16° isopycnic primitive equation model, a parallel version of the Miami Isopycnic Coordinate Ocean Model (Bleck and Smith 1990). The momentum and thickness diffusion have been modified to include biharmonic mixing in order to dissipate enstrophy near the grid scale, allowing large enstrophy gradients to emerge. The coefficients of thickness and momentum diffusivity are $A_h = (\Delta x)^3 \times 5 \times 10^{-3}$ m s$^{-1} \sim 1.25 \times 10^9$ m^4 s^{-1} and $A_u \geq (\Delta x)^3 \times 10^{-2}$ m s$^{-1} \sim 2.5 \times 10^9$ m^4 s^{-1}, respectively, the latter being in the form of Smagorinsky, deformation-dependent viscosity, where Δx is the grid spacing.

The model experiments are forced as a classical, wind-driven double gyre within a flat-bottom basin on a beta plane. The zonal wind stress is $\tau_x = -\tau_o \cos(2\pi y/L)$, where $\tau_o = 0.15$ N m^{-2} and L is the meridional basin scale. The domain extends from 14° to 36°N and spans 25° in longitude. There are vertical sidewalls with a free-slip boundary condition. Along the seafloor, there is a bottom drag, $\tau_b = -c_D(|\mathbf{u}_{\text{bot}}| + 0.01)\mathbf{u}_{\text{bot}}$, where the drag coefficient $c_D = 3 \times 10^{-3}$. Initial layer interfaces are at depths of 500, 1250, 2000, and 2750 m, and a seafloor is at 4000 m.

The model does not include a mixed layer, although an artificial diapycnic transfer is included to prevent outcropping. The diapycnal transfer is only activated when the surface layer becomes less than 10 m in thickness; the layer thickness is locally relaxed back to 10 m and, to conserve volume of the surface layer, the layer thickness is uniformly decreased over the rest of the domain by an appropriate amount. The vorticity equation is formulated to conserve PV and enstrophy even in the limit of layers having vanishing thickness (Boudra and Chassignet 1988).

The model is integrated for 25 yr and diagnostics are conducted over the initial 3 yr of the spinup period or over the last 10 yr when the model is close to a statistically steady state. For simplicity we focus on the evolution of an intermediate layer, because there is no direct influence of wind forcing or bottom drag.

b. Time-mean state

The time-mean state is evaluated here from diagnostics extending from years 15 to 25 (with enstrophy now evaluated over this 10-yr period). The depth-integrated transport reveals a midbasin jet separating from the western boundary at 22°N with a maximum transport that reaches 100 Sv (1 Sv $\equiv 10^6$ m^3 s^{-1}; Fig. 2a, contours). The jet separates a relatively strong subtropical gyre and weak subpolar gyre. Tightly confined recirculations also emerge against the northern and southern boundaries.

The PV is evaluated using a layer definition, $Q = (\zeta + f)/h$, where ζ is the relative vorticity, f is the planetary vorticity, and h is the layer thickness. All subsequent diagnostics are shown for an intermediate layer, layer 3, which is initially between interfaces at 1250 and 2000 m.

The time-mean PV reveals reduced PV contrasts over the gyre interior and enhanced gradients on the flanks of the combined subtropical and subpolar gyres (Fig. 2a). Along the gyre flanks, the flow is most unstable to baroclinic instability and instantaneous PV contours are, on average, preferentially deformed from their mean positions near the Rossby deformation scale. Thus, the time-mean enstrophy is relatively concentrated on the flanks of the combined subtropical and subpolar gyres (along 18° and 34°N), as well as along the western boundary (Fig. 2b). In the jet, the time-mean enstrophy is smaller because the horizontal shear deforms PV contours and enables the small-scale dissipation to remove enstrophy.

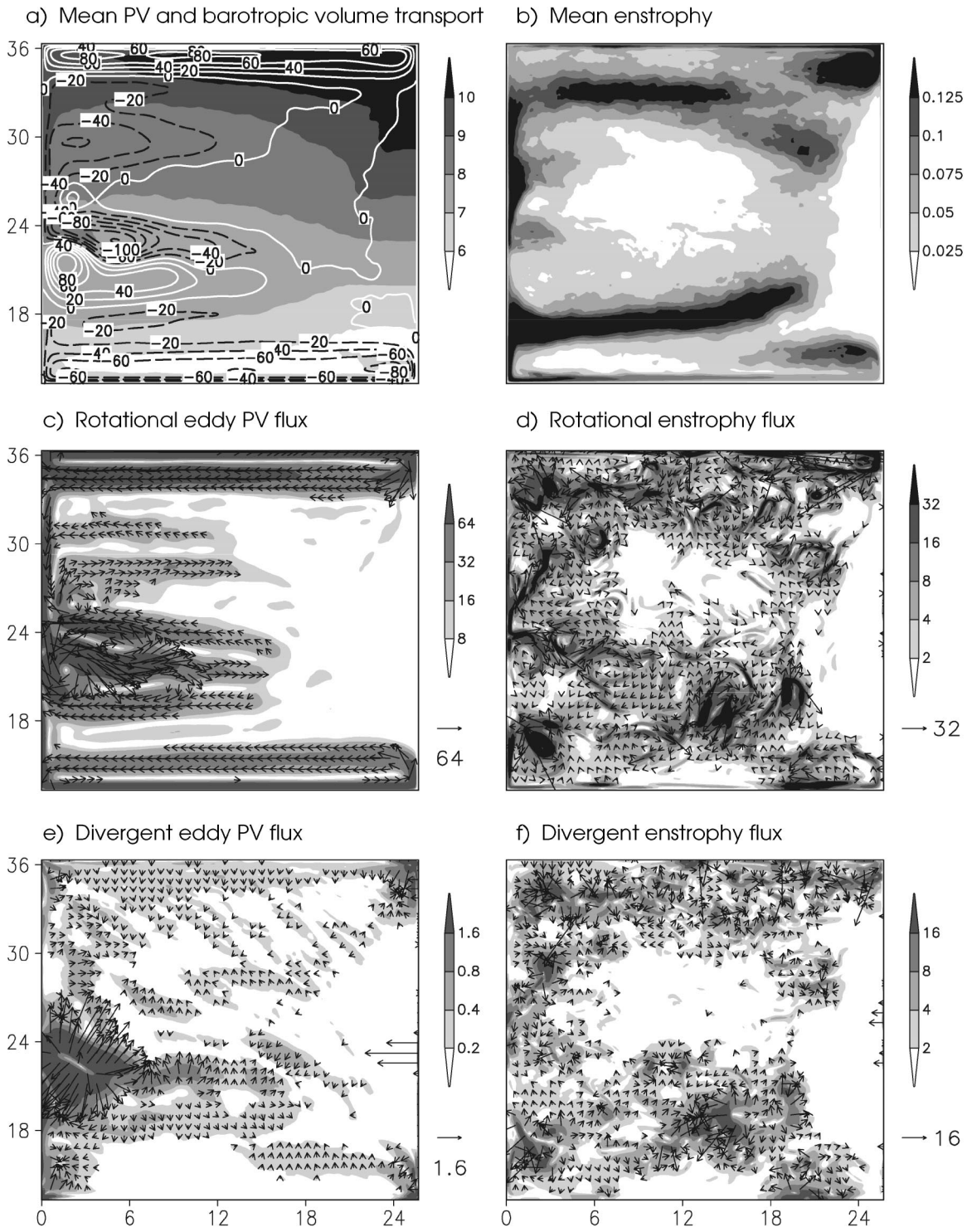

FIG. 2. Time-mean maps from years 15 to 25 for an intermediate layer (layer 3, initially between interfaces at 1250–2000 m): (a) PV (shaded) (10^{-8} m^{-1} s^{-1}), (b) enstrophy (10^{-16} m^{-2} s^{-2}), rotational component of the (c) eddy PV flux (10^{-10} s^{-2}) and (d) thickness-weighted enstrophy flux (10^{-18} s^{-3}), and divergent component of the (e) eddy PV flux (10^{-10} s^{-2}) and (f) thickness-weighted enstrophy flux (10^{-18} s^{-3}). In (a), the depth-integrated volume transport streamfunction (10^{6} m^{3} s^{-1}) is superimposed as contours. In (c)–(f), the shading denotes the magnitude of the vectors.

1) PV AND ENSTROPHY FLUXES

The PV and the enstrophy fluxes have contrasting patterns over the domain and differ in the relative importance of their rotational and divergent components, as by Roberts and Marshall (2000) with zero normal components on boundaries. For PV, the eddy flux $\overline{\mathbf{u}'Q'}$ is dominated by the rotational component, which is typically a factor of 10 larger than the divergent component (Figs. 2c,e). The rotational flux is concentrated over the central gyre recirculation, as well as along the recirculations adjacent to the northern and southern boundaries. The divergent flux instead is only significant over the northern boundary and the central gyre recirculation.

For the thickness-weighted enstrophy flux $\overline{h\mathbf{u}(Q'^2/2)}$, the rotational component is typically a factor of 1000 larger than the divergent component (Figs. 2d,f). The total flux is dominated by the eddy contribution; the total flux is shown, though, because it more closely relates to the flux form of the enstrophy budget shown later in (4). The pattern of the divergent enstrophy flux reflects the time-mean enstrophy distribution (Fig. 2b) with maxima along the flanks of the gyre recirculations and a minimum over the central part of the intergyre boundary.

2) PARAMETERIZATION OF EDDY THICKNESS AND PV FLUXES

The implied diffusivities for the eddy PV flux and, for completeness, the eddy thickness flux are diagnosed using the time-mean diagnostics, for years 15–25 (shown in Fig. 2). The diffusivities are diagnosed using the following downgradient closures:

$$\overline{\mathbf{u}'Q'} = -\kappa_Q \boldsymbol{\nabla}\overline{Q}, \qquad \overline{\mathbf{u}'h'} = -\kappa_h \boldsymbol{\nabla}\overline{h},$$

where κ is the implied eddy diffusivity for PV or thickness, as denoted by the subscript Q or h, respectively.

The diagnosed κ show large positive and negative values for both PV and thickness when evaluated either in terms of the total flux or only in terms of the divergent flux component (Fig. 3). The κ generally reach their largest magnitude along the midbasin jet and have smaller values elsewhere. There is a smoother structure for κ_h when compared with κ_Q, which is probably a consequence of the smoother distribution of h when compared with PV. However, the κ for both thickness and PV show positive and negative values, reflecting the up- and downgradient direction of the eddy fluxes.

Given the changing sign in κ, we now consider why these patterns emerge and how they are controlled. Rather than duplicate the discussion, we focus on the control of the eddy PV flux, because PV is the dynamically conserved tracer.

c. PV and enstrophy evolution

The evolution of the PV and enstrophy distributions are revealed in snapshots shown in Fig. 4. There initially is a linear gradient in PV with zonal contours over the basin. Advection of PV along the western boundary leads to large contrasts in PV being formed across the meandering midbasin jet, and instability of the jet generates an active eddy field (Fig. 4a, left panel). As the spinup progresses, the eddy stirring leads to the interior PV distribution becoming more uniform, with PV contours expelled toward the gyre flanks (Figs. 4b,c). This result is evident in how two time-mean PV contours, marked by solid lines in Fig. 4, gradually acquire a wider spacing over the spinup; the time averaging for this figure is based upon a 600-day window centered on the time of each snapshot. The PV adjustment occurs mainly over the first 6 yr, and there is little subsequent evolution in the time-mean PV.

The enstrophy evolves according to the changes in PV (Fig. 4, right panel); the enstrophy is defined here by the PV deviation from the running time average applied over the 600-day window. There initially is concentration of enstrophy along and in the vicinity of the midbasin jet, consisting of a heterogeneous organization of deformation-scale patches (Fig. 4a, right panel). The enstrophy eventually becomes concentrated along the gyre flanks (Figs. 4b,c) as the PV gradients become expelled from the interior.

The subsequent detailed evolution of the enstrophy at a statistically steady state is revealed in Fig. 5. The sequence starts with a magnified snapshot as seen in Fig. 4c between 16° and 27°N. Over a 40-day period, a long, thin patch of high enstrophy in the jet (Fig. 5a) is stretched by the horizontal shear until it is thin enough to be diffused (Figs. 5b,c). A large patch of high enstrophy, created along the gyre flank, is advected simultaneously along the western boundary and midbasin jet into the gyre interior (Figs. 5a–d).

This cycle of creation of patches of high enstrophy near the deformation scale and diffusion at the smallest scales is observed throughout the basin. Animations of the enstrophy distribution suggest that there is preferential formation of enstrophy along the gyre flanks and destruction along the midbasin jet.

d. Time-mean local budget of enstrophy

The dominant balance in the enstrophy budget [(1b)] is now examined in more detail locally over two periods, during the early part of the spinup from years 0 to 3 and at a statistically steady state from years 15 to 25:

$$\overline{\frac{\partial}{\partial t}\frac{Q'^2}{2}} + \overline{\overline{\mathbf{u}}\cdot\boldsymbol{\nabla}\frac{Q'^2}{2}} + \overline{\mathbf{u}'\cdot\boldsymbol{\nabla}\frac{Q'^2}{2}} + \overline{\mathbf{u}'Q'}\cdot\boldsymbol{\nabla}\overline{Q} = \overline{F'Q'},$$

where $\mathbf{u}$ is now taken as the velocity along the isopycnic layer.

For years 0–3, there is an oscillating pattern of up- and downgradient eddy PV fluxes, as revealed in the scalar product, $-\overline{\mathbf{u}'Q'}\cdot\boldsymbol{\nabla}\overline{Q}$, over much of the domain (Fig. 6a). This reversing pattern is locally controlled by

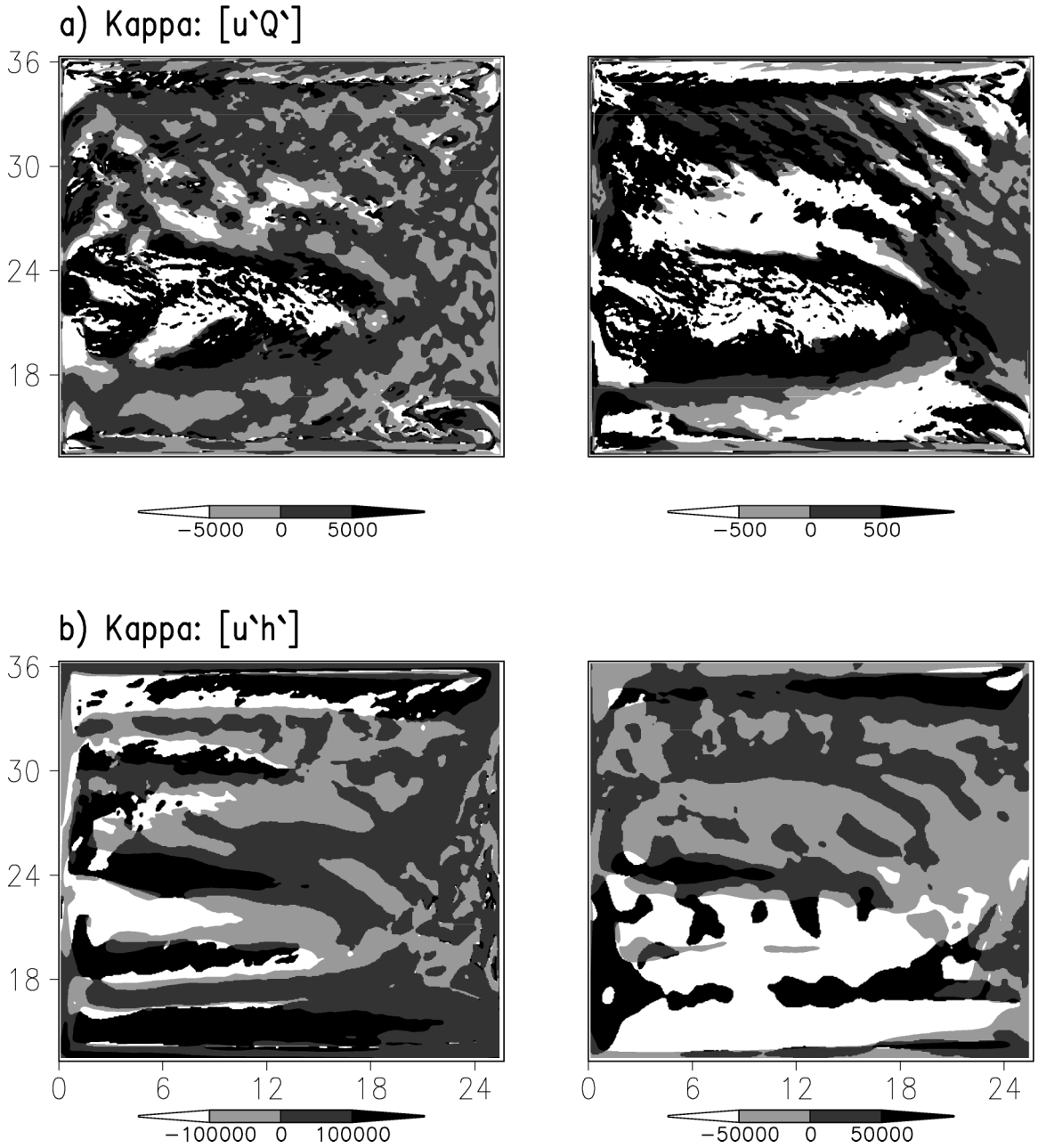

FIG. 3. The diagnosed eddy diffusivity ($m^2\ s^{-1}$) κ associated with two choices for downgradient closures in terms of (a) PV, $\overline{\mathbf{u}'Q'} = -\kappa_Q \nabla \overline{Q}$, and (b) thickness, $\overline{\mathbf{u}'h'} = -\kappa_h \nabla \overline{h}$. The diffusivities are diagnosed from the resolved eddy fluxes and time-mean gradients from years 15 to 25. The diffusivities are evaluated using (left) the total flux and (right) only its divergent component.

the advection of enstrophy, $\overline{\mathbf{u} \cdot \nabla (Q'^2/2)}$ (Fig. 6b). The residual of these terms is relatively small and is concentrated over the western boundary where the numerical diffusion and dissipation of enstrophy are relatively large.

For years 15–25, there is a similar balance between the advection of enstrophy and the scalar product of the eddy PV flux and the mean PV gradient. The main difference is that a larger-scale pattern for the downgradient eddy PV flux emerges with regions of downgradient flux concentrated along the gyre flanks (along 18° and 34°N in the experiments).

Given how the enstrophy advection controls the direction of the eddy PV flux, rather than temporal change in the enstrophy or explicit forcing or dissipation of enstrophy, the separate contributions of the advection by the time-mean and eddy flows are considered (Fig. 7). The enstrophy advection by the time-mean and eddy flows contain opposing finescale structure, because the fine structure does not appear for the total advection of

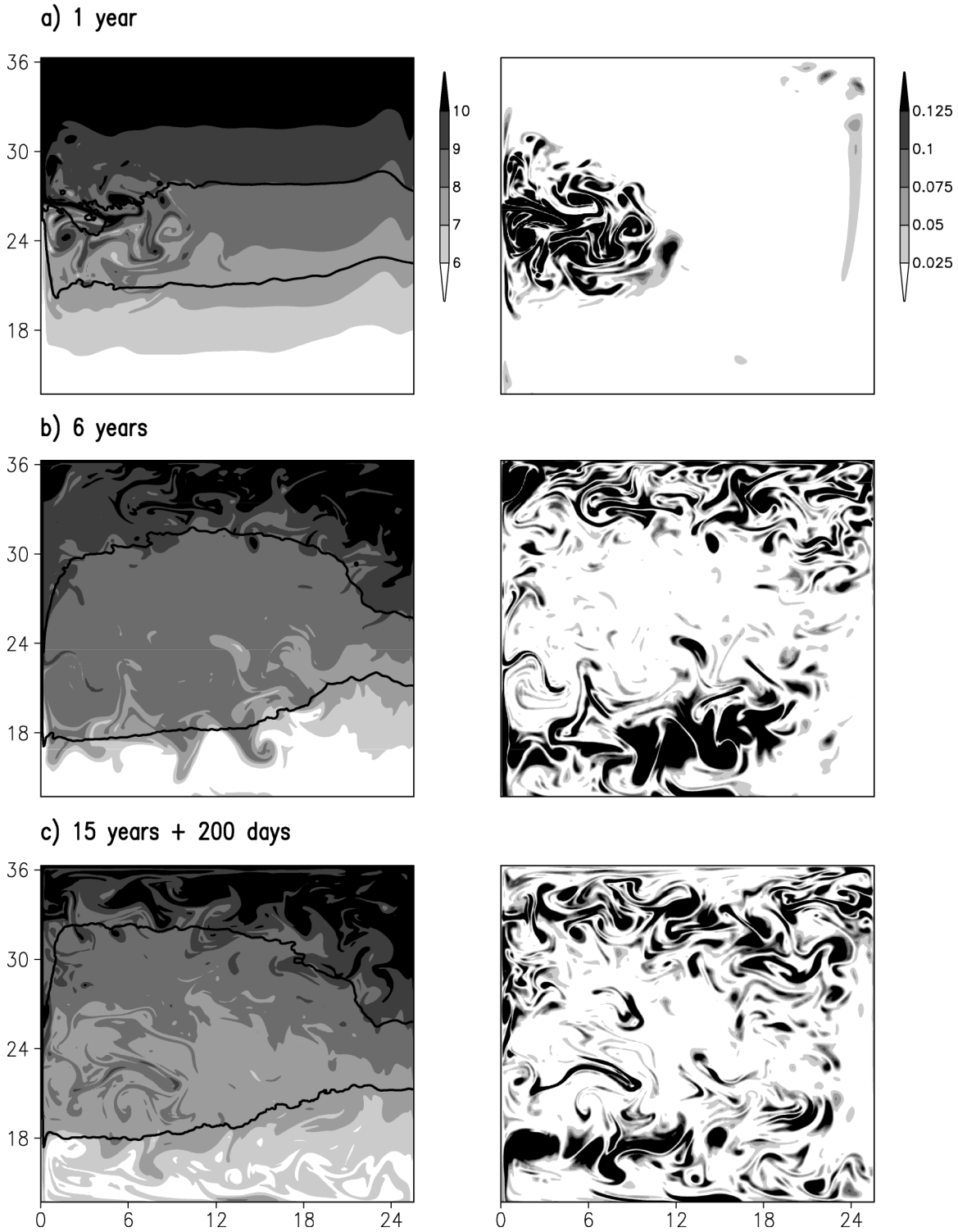

FIG. 4. Instantaneous maps of (left) PV (10^{-8} m^{-1} s^{-1}) and (right) eddy enstrophy (10^{-16} m^{-2} s^{-2}) for layer 3 during the model spinup and at equilibration: (a) 1 yr, (b) 6 yr, and (c) 15 yr + 200 days, respectively. The positions of two time-mean PV contours (7.5 and 9.0 $\times$ 10^{-8} m^{-1} s^{-1}) are denoted by thick lines, where the time averaging is applied as a windowed mean extending over a 600-day period centered at the time of the snapshot.

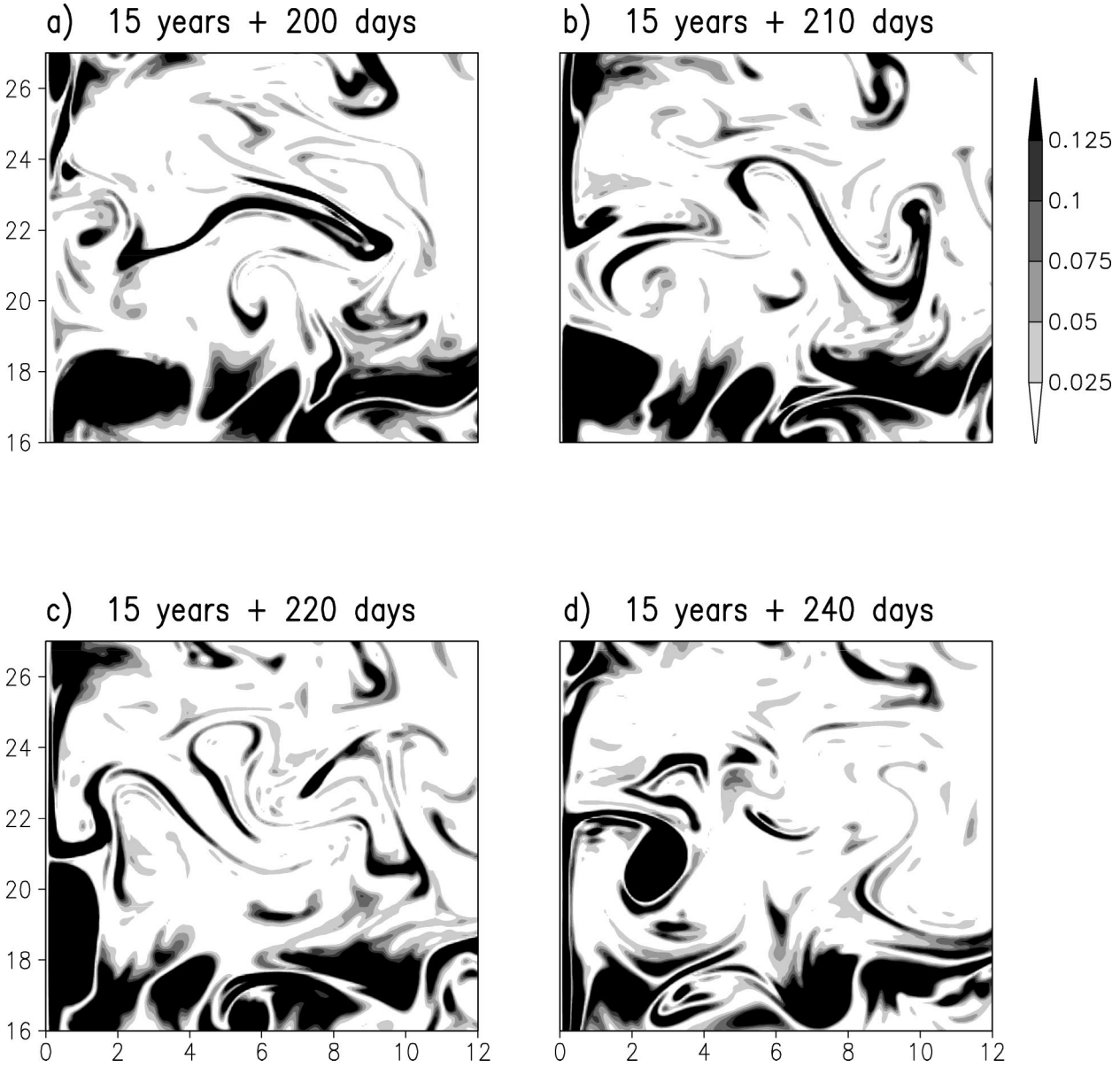

FIG. 5. Series of snapshots of enstrophy (10^{-16} m^{-2} s^{-2}) after 15 years at (a) 200, (b) 210, (c) 220, and (d) 240 days. In (a)–(c), a thin patch of high enstrophy in the jet at 22°N is stretched by the horizontal shear until it is thin enough to eventually be diffused. In (a)–(d), a large patch of high enstrophy, created in the gyre flank at 17°N, is advected along the western boundary and midbasin jet into the gyre interior.

enstrophy (Fig. 6b). However, the larger-scale patterns in the enstrophy advection (Fig. 6) are controlled by the contribution from the eddy advection of enstrophy (Fig. 7a) rather than by enstrophy advection by the time-mean flow (Fig. 7b).

e. Interpretation of dominant enstrophy balance

The time-mean of the scalar product of the eddy PV flux and the PV gradient [(2)] is given by

$$\overline{\mathbf{u}'Q'\cdot\nabla Q} \equiv \overline{\mathbf{u}'Q'}\cdot\nabla\overline{Q} + \overline{\mathbf{u}'Q'\cdot\nabla Q'} = \overline{\mathbf{u}'Q'}\cdot\nabla\overline{Q} + \overline{\mathbf{u}'\cdot\nabla\frac{Q'^2}{2}}.$$

Thus, the limit when the enstrophy budget [(1b)] reduces to

$$-\overline{\mathbf{u}'Q'}\cdot\nabla\overline{Q} \sim \overline{\mathbf{u}'\cdot\nabla\frac{Q'^2}{2}}$$

is equivalent to the eddy PV flux being *aligned* along the PV contours, $\overline{\mathbf{u}'Q'\cdot\nabla Q} = 0$ [(3*b*)]. In our model

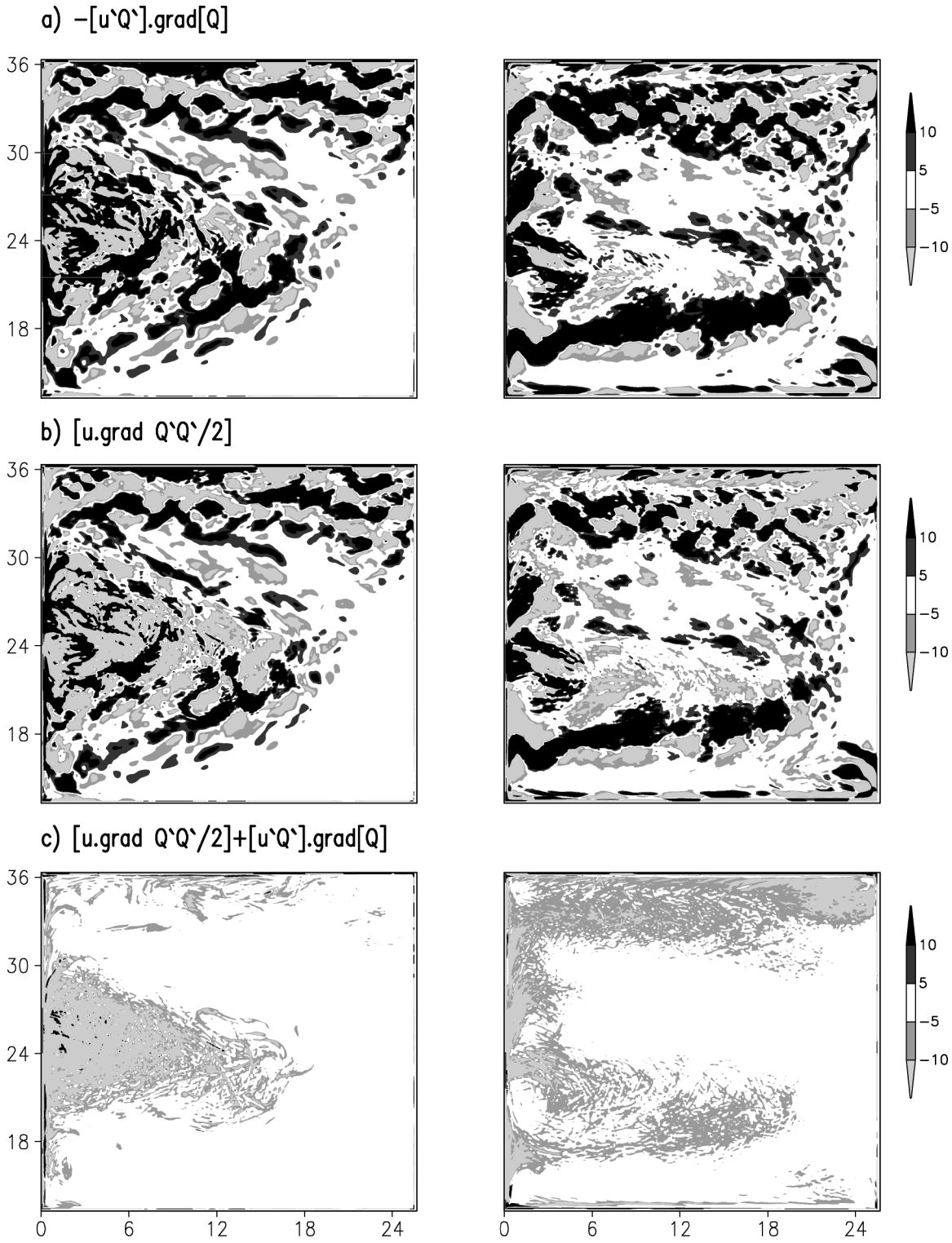

FIG. 6. Time-mean enstrophy budget (10^{-25} m^{-2} s^{-3}) for two time periods, (left) during spinup from years 0–3 and (right) years 15–25: (a) negative scalar product of the eddy PV flux and mean PV gradient, $-\overline{\mathbf{u}'Q'} \cdot \nabla\overline{Q}$; (b) advection of enstrophy, $\overline{\mathbf{u} \cdot \nabla(Q'^2/2)}$; (c) residual from (a) and (b). The shading denotes large positive and negative values as dark and light, respectively. The omitted terms for the temporal evolution, explicit forcing, and dissipation are negligible.

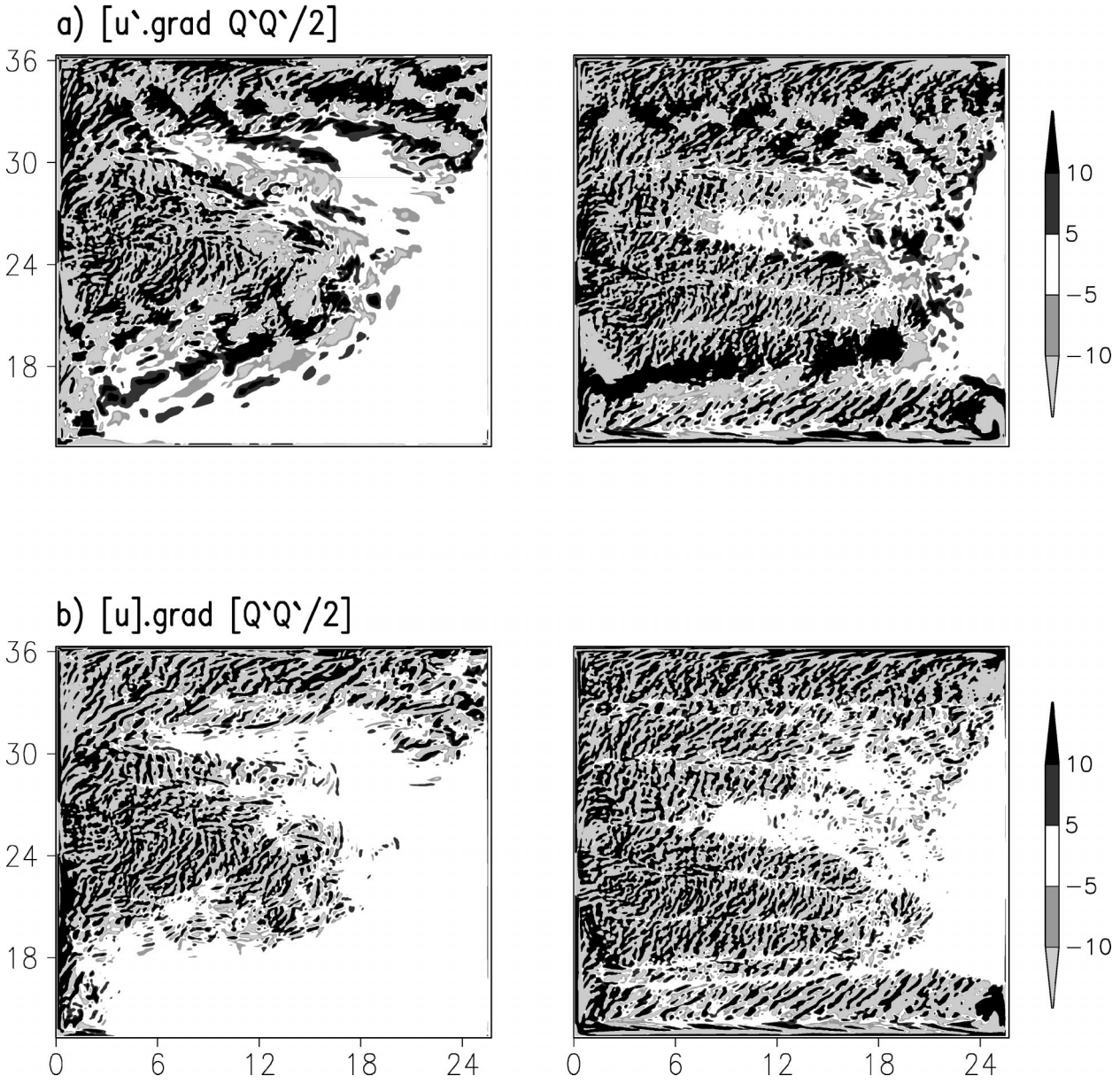

FIG. 7. Advection of enstrophy (10^{-25} m^{-2} s^{-3}) separated into the contributions from (a) eddy velocity $\overline{\mathbf{u}' \cdot \nabla(Q'^2/2)}$ and (b) the time-mean velocity $\overline{\mathbf{u}} \cdot \nabla\overline{(Q'^2/2)}$. The diagnostics are shown for two time periods, (left) during spinup from years 0–3 and (right) years 15–25.

diagnostics, this limit appears to apply, both at a statistically steady state for years 15–25 and in the earlier diagnostics at years 0–3, as depicted in Figs. 6 and 7.

We had expected a different balance during the spinup [(3a)] (see Fig. 1), when the eddy PV flux is expected to be directed downgradient and linked to an expelling of PV contours. However, our model diagnostics have not captured this signal, and it is probably difficult to achieve, because choosing an averaging period that is too short does not provide reliable diagnostics and choosing an averaging period that is too long leads to the initial signal being masked.

f. Time-mean flux form of the enstrophy budget

The enstrophy budget [(1b)] is now diagnosed in its flux form (see appendix) with a time average from years 15 to 25:

$$\overline{\frac{1}{h}\frac{\partial}{\partial t}\left(h\frac{Q'^2}{2}\right)} + \overline{\frac{1}{h}\nabla\cdot\left(\mathbf{u}h\frac{Q'^2}{2}\right)} + \overline{\mathbf{u}'Q'}\cdot\nabla\overline{Q} = \overline{F'Q'} + \overline{\frac{D_h}{h}\frac{Q'^2}{2}}. \quad (4)$$

The downgradient eddy PV flux is controlled by the

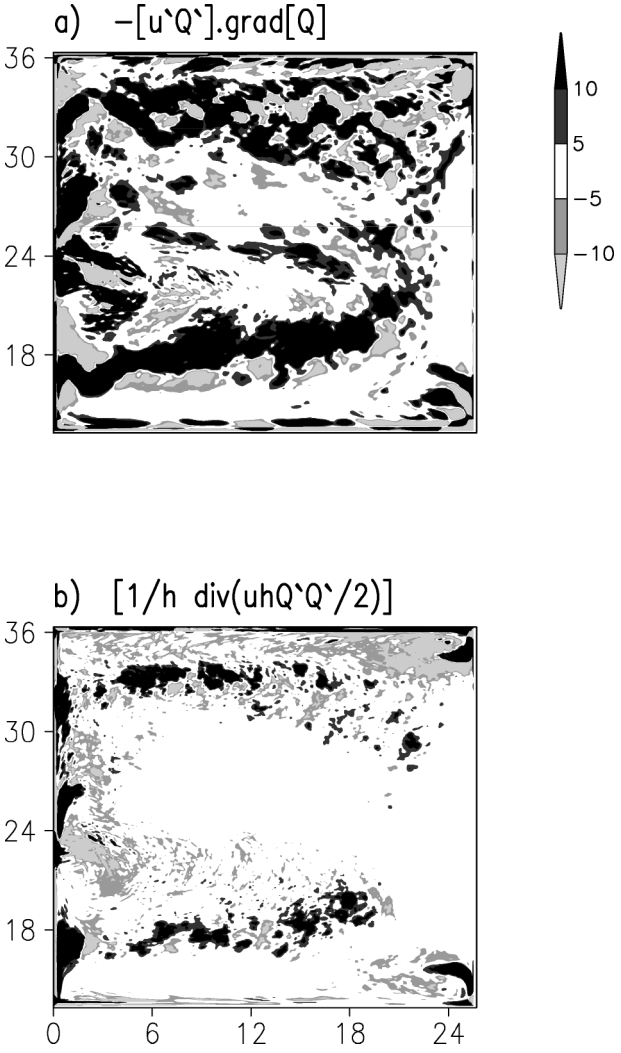

FIG. 8. Diagnostics from the flux form of the enstrophy budget (10^{-25} m^{-2} s^{-3}) for years 15–25: (a) negative scalar product of the eddy PV flux and mean PV gradient, $-\overline{\mathbf{u}'Q'} \cdot \boldsymbol{\nabla}\overline{Q}$, and (b) weighted divergence of the flux of enstrophy, $\overline{(1/h)\boldsymbol{\nabla} \cdot (\mathbf{u}h)(Q'^2/2)}$.

divergence of the flux of enstrophy, with the dominant balance in (4) given by

$$\overline{\mathbf{u}'Q'} \cdot \boldsymbol{\nabla}\overline{Q} \sim -\overline{\frac{1}{h}\boldsymbol{\nabla} \cdot \left(\mathbf{u}h\frac{Q'^2}{2}\right)},$$

as revealed in Figs. 8a,b. In practice, diagnostics of $\overline{(1/h)\boldsymbol{\nabla} \cdot [\mathbf{u}h(Q'^2/2)]}$ are identical to those of $(1/h)\boldsymbol{\nabla} \cdot \overline{[\mathbf{u}h(Q'^2/2)]}$.

The large-scale patterns in the eddy PV flux show a downgradient flux along the gyre flanks and an upgradient flux over the midbasin jet. At a statistically steady state, these regions correspond to source and sink regions for enstrophy; enstrophy is created through baroclinic instability along the gyre flanks and is dissipated in a region of strong velocity shear along the midbasin jet. The flux form of the enstrophy budget emphasizes how these sources and sinks of enstrophy are connected by a thickness-weighted flux of enstrophy, $\mathbf{u}h(Q'^2/2)$. However, although this interpretation might be plausible, the large rotational flux of enstrophy obscures this picture of a simple advective transfer between sources and sinks of enstrophy (Fig. 2d).

g. Scaling of advective terms in the enstrophy budget

Our model diagnostics suggest that, at a statistically steady state, the eddy PV flux is directed down- or upgradient according to the sign of the advection of enstrophy, with the eddy advection playing a dominant role. In contrast, previous quasigeostrophic studies, such as Holland and Rhines (1980) and Marshall and Shutts (1981), explained the eddy PV flux in terms of enstrophy dissipation and the advection by the time-mean flow. Given our contrasting results, we further examine the scaling necessary for our balances.

The ratio of the eddy advection of enstrophy to the scalar product of eddy PV flux and mean PV gradient is typically of order 1 in our model diagnostics (Fig. 9a). Applying scale analysis, this ratio is approximately related to a ratio of length scales

$$\left|\frac{\overline{\mathbf{u}' \cdot \boldsymbol{\nabla}\dfrac{Q'^2}{2}}}{\overline{\mathbf{u}'Q'} \cdot \boldsymbol{\nabla}\overline{Q}}\right| \sim \frac{L_{\overline{Q}}}{L_{Q'}}, \tag{5}$$

where $L_{\overline{Q}} \sim |(\overline{Q'^2})^{1/2}/\boldsymbol{\nabla}\overline{Q}|$ and $L_{Q'} \sim |(\overline{Q'^2})^{1/2}/\boldsymbol{\nabla}[(\overline{Q'^2})^{1/2}]|$ reflect the length scales over which the enstrophy varies relative to the horizontal gradients in mean PV and perturbation PV (the latter defined from the square root of enstrophy). The ratio of these length scales is again typically of order 1 (Fig. 9b), suggesting that the scale over which the enstrophy varies is several 100 km (Fig. 9c); note that Figs. 9a and 9b do not simply reflect each other because of the scalar products in (5).

The advection of enstrophy by the mean and eddy flow is comparable on a finescale. However, on a larger regional scale, the advection by the mean flow does not make a significant contribution. Thus, the magnitude of the ratio of the mean advection of enstrophy to the scalar product of eddy PV flux and mean PV gradient is typically smaller than 1 in our model diagnostics (Figs. 6b and 7b). Applying scale analysis, this ratio is given by

$$\frac{\overline{\overline{\mathbf{u}} \cdot \boldsymbol{\nabla}\dfrac{Q'^2}{2}}}{\overline{\mathbf{u}'Q'} \cdot \boldsymbol{\nabla}\overline{Q}} \sim \frac{L_{\overline{Q}}}{L_{Q'}}\frac{|\overline{\mathbf{u}}|}{|\mathbf{u}'|}, \tag{6}$$

where $|\mathbf{u}'| \equiv (\overline{u'^2} + \overline{v'^2})^{1/2}$. The relative smallness of this ratio is due to the magnitude of the mean velocity $|\overline{\mathbf{u}}|$ being a factor of 2–4 smaller than the eddy velocity $|\mathbf{u}'|$ for this middepth layer (Fig. 9d). In other model studies, possibly different advective balances might emerge in the enstrophy budget through changes in these nondimensional ratios, $L_{\overline{Q}}/L_{Q'}$ and $|\overline{\mathbf{u}}|/|\mathbf{u}'|$ (arising

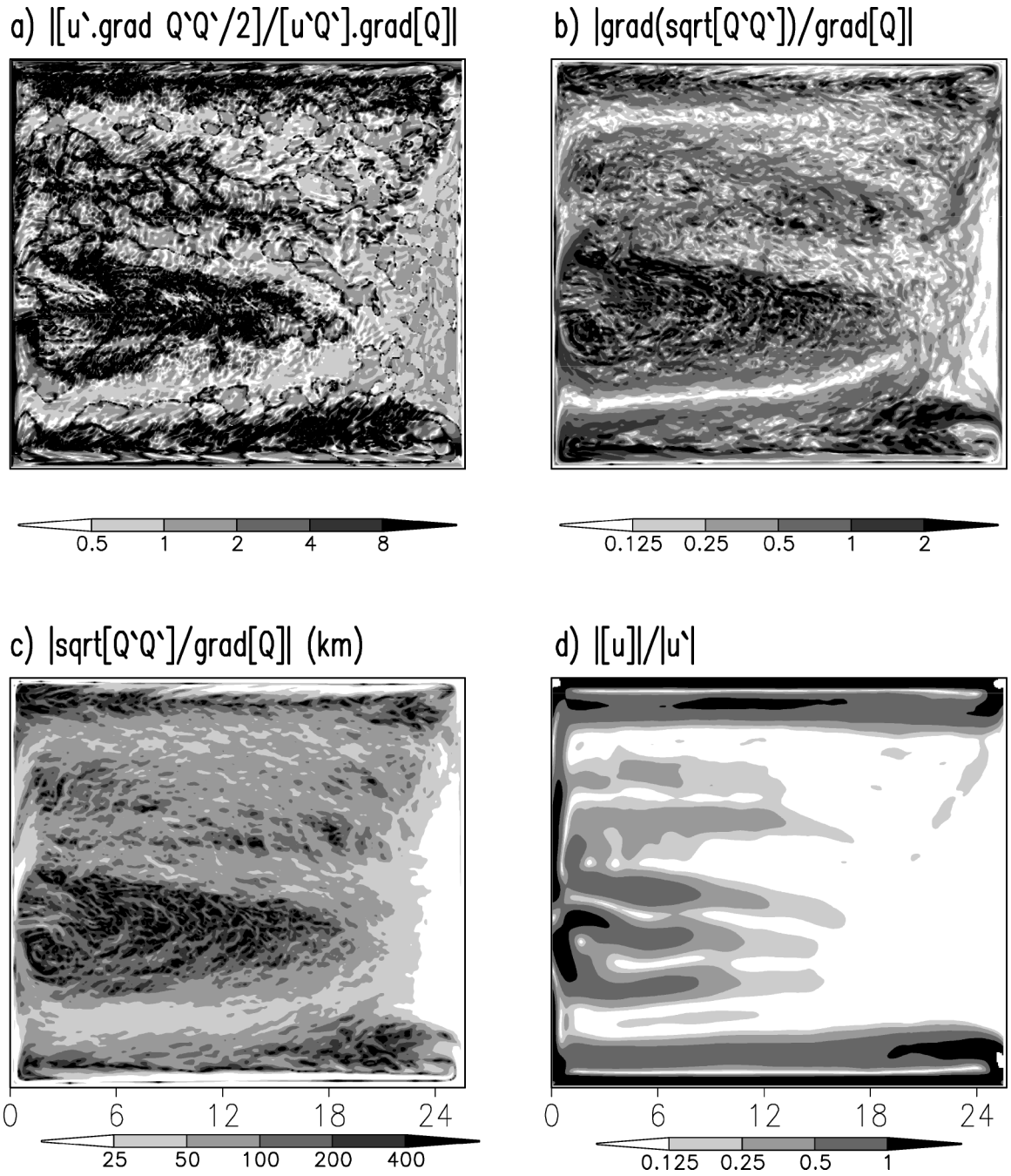

FIG. 9. (a) Ratio of magnitudes of eddy advection of enstrophy, $|\overline{\mathbf{u}' \cdot \nabla(Q'^2/2)}|$, and scalar product of the eddy PV flux and mean PV gradient, $|\overline{\mathbf{u}'Q'} \cdot \nabla\overline{Q}|$. (b) Ratio of length scales $L_{\overline{Q}}/L_{Q'}$, where each length scale measures the scale over which the enstrophy varies relative to the mean PV gradient, $L_{\overline{Q}} \sim |(\overline{Q'^2})^{1/2}/\nabla\overline{Q}|$, and the gradient in the perturbation PV, $L_{Q'} \sim |(\overline{Q'^2})^{1/2}/\nabla[(\overline{Q'^2})^{1/2}]|$. (c) Length scale over which enstrophy varies relative to the mean PV gradient (km) $L_{\overline{Q}}$, which is typically several 100 km. (d) Ratio of magnitudes of mean velocity and eddy velocity, $|\overline{\mathbf{u}}|/|\mathbf{u}'|$, where $|\mathbf{u}'| = (\overline{u'^2} + \overline{v'^2})^{1/2}$.

from different choices in the model domain, resolution, or forcing).

4. Discussion

Eddies affect the time-mean circulation through their systematic transfer of dynamic tracers. For example, PV is homogenized within closed geostrophic streamlines by eddy stirring. However, despite this systematic effect, model tests of eddy parameterization schemes based on downgradient closures have been inconclusive.

In this study, we consider the connection between the

evolution and advection of enstrophy and the eddy PV flux [(1a)]:

$$\overline{\frac{D}{Dt}\frac{Q'^2}{2}} + \overline{\mathbf{u}'Q'} \cdot \boldsymbol{\nabla}\overline{Q} = \overline{F'Q'},$$

where there is a three-way balance between the Lagrangian evolution of enstrophy, the scalar product of the eddy PV flux and the PV gradient, and the forcing of enstrophy. This relationship suggests that the following regimes might occur:

1) When there is an area-average increase in enstrophy within a closed streamline, the eddy PV flux should be directed, on average, downgradient. This regime should occur during the spinup of an ocean basin where the increase in enstrophy is concomitant with the expulsion of PV contours within closed geostrophic streamlines.
2) Enstrophy concentrations become high on the gyre flanks and low over the gyre interior. This pattern implies that there should be a Lagrangian increase in enstrophy as fluid moves onto the gyre flanks, leading to a downgradient eddy PV flux, and a Lagrangian decrease of enstrophy as fluid moves off the flanks, leading to an upgradient eddy PV flux.

In our eddy-resolving diagnostics, the Lagrangian evolution of enstrophy is controlled by the advection of enstrophy, rather than by forcing or dissipation of enstrophy. Locally, the advection of enstrophy leads to reversing patterns of up- and downgradient eddy PV fluxes. At a statistically steady state, large-scale patterns of downgradient eddy PV flux only emerge along the flanks of the gyre and part of the western boundary, associated with the high levels of enstrophy there. These large-scale patterns of the eddy PV flux are controlled by the eddy advection of enstrophy, rather than by the advection by the time-mean flow. As a consequence, at a statistically steady state, this dominance of eddy advection of enstrophy suggests that the eddy PV flux is locally controlled by intrinsic wave properties, rather than reflecting any control of the gyre-scale circulation. The large PV gradients along the gyre flanks are possibly acting as waveguides. The time-mean flow is, however, still ultimately important in shaping the PV and enstrophy distributions.

The crucial issue for any eddy parameterization scheme is determining which aspect of eddy behavior it is designed to replicate. Our model diagnostics suggest that attempting to simulate the detailed pattern of eddy fluxes is problematic, particularly at a statistically steady state, because of the importance of eddy advection in shaping these patterns. Neither a thickness nor a PV closure scheme is likely to succeed, because eddy advection does not depend soley on larger-scale, time-mean variables.

Instead, in our view, the preferable objective is to devise a parameterization scheme that captures the evolution of time-mean variables, rather than simulating the detail of the eddy fluxes. For this more limited objective of capturing the large-scale evolution, a downgradient PV closure appears preferable to a thickness closure, because PV is a materially conserved quantity and eddy-resolving models show PV being homogenized, rather than layer thickness. A more satisfying theoretical extension might be to relax the requirement that the eddy flux is always downgradient and instead allow the parameterized fluxes to be directed downgradient where enstrophy is created and upgradient where enstrophy is destroyed following the flow.

Acknowledgments. The work was supported by the UK NERC COAPEC program (NER/T/S/2000/00305) and an HEFCE JREI award in 1999 for a supercomputing cluster (NESSC). We are grateful to Isaac Held for an insightful review, which strengthened this study. We thank Vassil Roussenov for assistance with the modeling studies and Richard Greatbatch, Chris Hughes, and David Marshall for useful discussions.

APPENDIX

The General Enstrophy Equation

The eddy potential enstrophy equation is derived generally following Rhines and Holland (1979), but including additional terms associated with horizontal divergence within a density layer (Drijfhout and Hazeleger 2001), and retaining terms involving third-order and higher eddy correlations.

The PV equation is given by

$$\frac{DQ}{Dt} = F, \tag{A1}$$

where $D/Dt = \partial/\partial t + \mathbf{u} \cdot \boldsymbol{\nabla}$, Q is the PV (Ertel or quasigeostrophic), F represents the forcing and dissipation of PV, and $\mathbf{u}$ is the three-dimensional velocity. Applying a time mean to (A1) gives

$$\frac{\partial\overline{Q}}{\partial t} + \overline{\mathbf{u} \cdot \boldsymbol{\nabla} Q} = \overline{F}, \tag{A2}$$

where a variable is written in the form $\alpha = \overline{\alpha} + \alpha'$, with $\overline{\alpha}$ being the average of α and $\overline{\alpha'} = 0$. Subtracting (A2) from (A1), the perturbed PV equation follows:

$$\frac{\partial Q'}{\partial t} + \mathbf{u} \cdot \boldsymbol{\nabla} Q' + \mathbf{u}' \cdot \boldsymbol{\nabla}\overline{Q} - \overline{\mathbf{u}' \cdot \boldsymbol{\nabla} Q'} = F'. \tag{A3}$$

To obtain the enstrophy equation, we now multiply (A3) by Q' and repeat the averaging operation, remembering that $\overline{\overline{\alpha}} = \overline{\alpha}$, and $\overline{\beta'\overline{\alpha}} = 0$, and also that $Q'\mathbf{u} \cdot \boldsymbol{\nabla} Q' = \mathbf{u} \cdot \boldsymbol{\nabla}(Q'^2/2)$:

$$\overline{\frac{\partial}{\partial t}\left(\frac{Q'^2}{2}\right)} + \overline{\mathbf{u} \cdot \boldsymbol{\nabla}\left(\frac{Q'^2}{2}\right)} + \overline{\mathbf{u}'Q'} \cdot \boldsymbol{\nabla}\overline{Q} = \overline{F'Q'}. \tag{A4}$$

This balance simplifies to a Lagrangian expression that relates the rate of change of eddy potential enstrophy

following the flow with the upgradient eddy potential vorticity flux and forcing of eddy enstrophy:

$$\overline{\frac{D}{Dt}\left(\frac{Q'^2}{2}\right)} + \overline{\mathbf{u}'Q'} \cdot \boldsymbol{\nabla}\overline{Q} = \overline{F'Q'}. \tag{A5}$$

To derive a flux form of the enstrophy equation, we take (A3) and multiply by hQ',

$$h\frac{\partial}{\partial t}\left(\frac{Q'^2}{2}\right) + \mathbf{u}h \cdot \boldsymbol{\nabla}\left(\frac{Q'^2}{2}\right) + h\mathbf{u}'Q' \cdot \boldsymbol{\nabla}\overline{Q} - hQ'\overline{\mathbf{u}' \cdot \boldsymbol{\nabla}Q'} = hQ'F', \tag{A6}$$

and also take the continuity equation,

$$\frac{\partial h}{\partial t} + \boldsymbol{\nabla} \cdot (\mathbf{u}h) = D_h, \tag{A7}$$

where D_h is the thickness dissipation, and multiply (A7) by $Q'^2/2$:

$$\frac{Q'^2}{2}\frac{\partial h}{\partial t} + \frac{Q'^2}{2}\boldsymbol{\nabla} \cdot (\mathbf{u}h) = D_h\frac{Q'^2}{2}, \tag{A8}$$

and then, by adding (A6) and (A8) and dividing by h, we obtain

$$\frac{1}{h}\frac{\partial}{\partial t}\left(h\frac{Q'^2}{2}\right) + \frac{1}{h}\boldsymbol{\nabla} \cdot \left(\mathbf{u}h\frac{Q'^2}{2}\right) + \mathbf{u}'Q' \cdot \boldsymbol{\nabla}\overline{Q} - Q'\overline{\mathbf{u}' \cdot \boldsymbol{\nabla}Q'} = F'Q' + \frac{D_h}{h}\frac{Q'^2}{2}. \tag{A9}$$

The flux form follows by taking the time mean of (A9):

$$\overline{\frac{1}{h}\frac{\partial}{\partial t}\left(h\frac{Q'^2}{2}\right)} + \overline{\frac{1}{h}\boldsymbol{\nabla} \cdot \left(\mathbf{u}h\frac{Q'^2}{2}\right)} + \overline{\mathbf{u}'Q'} \cdot \boldsymbol{\nabla}\overline{Q} = \overline{F'Q'} + \overline{\frac{D_h}{h}\frac{Q'^2}{2}}. \tag{A10}$$

REFERENCES

Bleck, R., and L. T. Smith, 1990: A wind-driven isopycnic coordinate model of the North and equatorial Atlantic Ocean. 1. Model development and supporting experiments. *J. Geophys. Res.,* **95,** 3273–3285.

Boudra, D. B., and E. P. Chassignet, 1988: Dynamics of Agulhas retroflection and ring formation in a numerical model. Part I: The vorticity balance. *J. Phys. Oceanogr.,* **18,** 280–303.

Drijfhout, S. S., and W. Hazeleger, 2001: Eddy mixing of potential vorticity versus thickness in an isopycnic ocean model. *J. Phys. Oceanogr.,* **31,** 481–505.

Gent, P. R., and J. C. McWilliams, 1990: Isopycnal mixing in ocean circulation models. *J. Phys. Oceanogr.,* **20,** 150–155.

——, J. Willebrand, T. J. McDougall, and J. C. McWilliams, 1995: Parameterizing eddy-induced tracer transports in ocean circulation models. *J. Phys. Oceanogr.,* **25,** 463–474.

Greatbatch, R. J., 1998: Exploring the relationship between eddy-induced transport velocity, vertical momentum transfer, and the isopycnal flux of potential vorticity. *J. Phys. Oceanogr.,* **28,** 422–432.

Holland, W. R., and P. B. Rhines, 1980: An example of eddy induced ocean circulation. *J. Phys. Oceanogr.,* **10,** 1010–1031.

Keffer, T., 1985: The ventilation of the world's oceans: Maps of the potential vorticity field. *J. Phys. Oceanogr.,* **15,** 509–523.

Killworth, P. D., 1997: On the parameterisation of eddy transfer. Part I: Theory. *J. Mar. Res.,* **55,** 1171–1197.

Lee, M.-M., D. P. Marshall, and R. G. Williams, 1997: On the eddy transfer of tracers: Advective or diffusive? *J. Mar. Res.,* **55,** 1–24.

Marshall, D. P., R. G. Williams, and M.-M. Lee, 1999: The relation between eddy-induced transport and isopycnic gradients of potential vorticity. *J. Phys. Oceanogr.,* **29,** 1571–1578.

Marshall, J. C., 1984: Eddy-mean flow interaction in a barotropic ocean model. *Quart. J. Roy. Meteor. Soc.,* **110,** 573–590.

——, and G. J. Shutts, 1981: A note on rotational and divergent eddy fluxes. *J. Phys. Oceanogr.,* **11,** 1677–1680.

McDowell, S., P. B. Rhines, and T. Keffer, 1982: North Atlantic potential vorticity and its relation to the general circulation. *J. Phys. Oceanogr.,* **12,** 1417–1436.

Peterson, K. A., and R. J. Greatbatch, 2001: Vorticity fluxes in shallow water ocean models. *Atmos.–Ocean,* **39,** 1–14.

Rhines, P. B., and W. R. Holland, 1979: A theoretical discussion of eddy-driven mean flows. *Dyn. Atmos. Oceans,* **3,** 289–325.

——, and W. R. Young, 1982a: Homogenization of potential vorticity in planetary gyres. *J. Fluid Mech.,* **122,** 347–368.

——, and ——, 1982b: A theory of the wind-driven circulation, I. Mid-ocean gyres. *J. Mar. Res.,* **40** (Suppl.), 559–596.

Roberts, M. J., and D. M. Marshall, 2000: On the validity of downgradient eddy closures in ocean models. *J. Geophys. Res.,* **105,** 28 613–28 627.

Treguier, A. M., I. M. Held, and V. D. Larichev, 1997: On the parameterization of quasigeostrophic eddies in primitive equation ocean models. *J. Phys. Oceanogr.,* **27,** 567–580.

Visbeck, M., J. Marshall, T. Haine, and M. Spall, 1997: On the specification of eddy transfer coefficients in coarse resolution ocean circulation models. *J. Phys. Oceanogr.,* **27,** 381–402.